Chinese Chemical Letters 34 (2023) 108005

Contents lists available at ScienceDirect

Chinese Chemical Letters

journal homepage: www.elsevier.com/locate/cclet

The self-assembly and structural regulation of a hydrogen-bonded dimeric building block formed by two N–H···O hydrogen bonds on HOPG

Peng Lei[a,c,1], Lin Ma[a,b,1], Siqi Zhang[a], Jianqiao Li[a,b], Linlin Gan[a,b], Ke Deng[a,*], Wubiao Duan[b,*], Wei Li[d,*], Qingdao Zeng[a,c,*]

[a] CAS Key Laboratory of Standardization and Measurement for Nanotechnology, CAS Center for Excellence in Nanoscience, National Center for Nanoscience and Technology (NCNST), Beijing 100190, China
[b] Department of Chemistry, School of Science, Beijing Jiaotong University, Beijing 100044, China
[c] Center of Material Science and Optoelectonics Engineering, University of Chinese Academy of Sciences, Beijing 100049, China
[d] School of Science, Nanchang Institute of Technology, Nanchang 330099, China

ARTICLE INFO

Article history:
Received 30 October 2022
Accepted 13 November 2022
Available online 17 November 2022

Keywords:
Self-assembly
Regulation
Scanning tunneling microscopy
DFT calculations
Co-assemble

ABSTRACT

The self-assembled behavior of an unsymmetric molecule (BCDTDA) with one imidazole group as center and benzoic acid group as functional group is studied, and the regulatory behaviors of coronene (COR) and three bipyridine derivatives (named BP, PEBP-C4 and PEBP-C8) on BCDTDA self-assembly structures are also investigated. Based on highly oriented pyrolytic graphite (HOPG) substrate, scanning tunneling microscopy (STM) is used to observe the variation of assembled behaviors at the solid-liquid interface. Because of the concentration effect, BCDTDA molecules can assemble into grids and Kagomés structures in the form of N–H···O hydrogen bonded dimers. BCDTDA molecules still maintain dimeric structures in the regulation of COR and BP molecules to BCDTDA self-assembly. However, PEBP-C4 and PEBP-C8 destroy the structure of the dimers, and form a variety of co-assembled structures with BCDTDA. Different guest molecules coordinate the host molecules differently, which makes the experiment more meaningful. Combined with density functional theory (DFT) calculation, the discovery of molecular interactions provides a promising strategy for the construction of functional nanostructures and devices.

Intermolecular interactions are the kernel of supramolecular chemistry [1–4]. More and more studies related to two-dimensional (2D) surface self-assembly, regarding the common hydrogen bonds [5–7], halogen bonds [8–10] and van der Waals interactions [11–13] as the main intermolecular forces, have been conducted. Due to the diversity and directionality of hydrogen bonding, it has the advantages of predictability and reversibility in dynamic behavior, which can optimize its performance and attract extensive attention of scientists [14–17]. If the process of self-assembly is well controlled, the goal of obtaining materials with specific structures and functions will be realized [18–21]. Organic compounds with carboxyl functional groups, which are widely used in photoelectric functional materials, are more likely to self-assemble at the 2D interface because of the provided binding sites for hydrogen bonding by carboxyl substituents [21–24]. Scanning tunneling microscopy (STM) is used not only to observe the formative ordered arrangement at the solid/liquid 2D interface, but also to fabricate the advanced on-surface devices [15,25-30].

Imidazole is a five-membered heterocyclic compound with two sites of N atoms, one of which has a lone pair of electrons and so it is easy to form hydrogen bonds. Imidazole derivatives show good luminescence properties and fluorescence quantum yield as a kind of super columnar liquid crystals [31,32]. Therefore, there are wide application prospects in the fields of organic electroluminescence materials, linear luminescence materials and other luminescence materials [33]. The host grid constructed by functional organic small molecules can flexibly adjust structures through the break and generation of non-covalent bonds, which is more conducive to the co-adsorption of guest molecules in the host molecular architecture.

The compound containing an imidazole group and oxygen—contained functional groups can form N–H···O hydrogen bonds in self-assembled structures, which is rarely investigated. Peng

* Corresponding authors.
E-mail addresses: kdeng@nanoctr.cn (K. Deng), wbduan@bjtu.edu.cn (W. Duan), liweidting@nit.edu.cn (W. Li), zengqd@nanoctr.cn (Q. Zeng).
[1] These authors contributed equally to this work.

https://doi.org/10.1016/j.cclet.2022.108005
1001-8417/

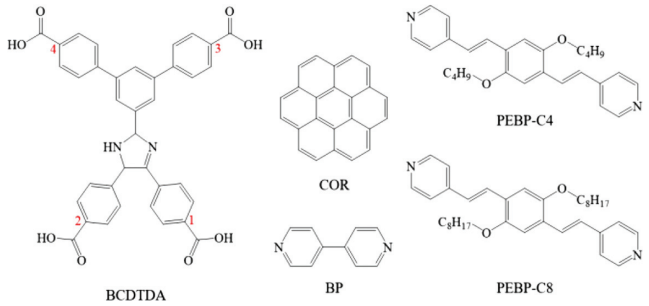

Scheme 1. The chemical structure of BCDTDA, COR, BP, PEBP-C4 and PEBP-C8, respectively.

et al. [7] have studied the self-assembly behaviours of 1,3,5-tri(1*H*-benzo[*d*]imidazol-2-yl) benzene (BTIB) with three imidazole groups. Despite the presence of imidazole groups, the BTIB molecule assembled into self-assembly structure through π-π stacking intermolecular forces and the N atoms of imidazole were exposed at the interface of 1-phenyloctane/HOPG. When one compound containing a carboxyl group is added as a guest molecule, BTIB can form O–H···N and N–H···O hydrogen bonds with it. Further study can greatly improve the insight into assembled structures of the compounds containing an imidazole group and provide strong evidence for designing specific molecular devices on 2D surfaces [34–36]. Generally speaking, the regulation of bi-pyridine and coronene (COR) molecules on single-molecule nano-grid structure is considered to be a good strategy [37–39], but there are few reports about self-assembled structural regulation of the dimers formed by hydrogen bonds. Zhang *et al.* [40] have successfully used pyridine derivatives to regulate self-assembled structure of the dimers formed by O–H···O hydrogen bonds. However, they used COR to regulate self-assembled structure of the dimers with no success. Moreover, the original host molecule aromatic pentacarboxylic acid (H_5BHB) always keeps self-assembled structures of the dimers in the process of regulation, but our results are different and innovative by maintaining the original dimeric structures selectively.

In this work, the self-assembled structure of an unsymmetric molecule 5′-(4,5-bis(4-carboxyphenyl)−2,5-dihydro-1*H*-imidazole-2-yl)-[1,1′:3′,1″-terphenyl]−4,4″-dicarboxylic acid (BCDTDA) was studied. BCDTDA molecule has four benzoic acid substituent groups in both ends and one imidazole group as a core. Furthermore, we used COR and three bi-pyridine molecules to execute the regulation of the BCDTDA self-assembled structures, and three bi-pyridine molecules are 4,4′-bipyridine (BP), 4,4′-((1*E*,1′*E*)-(2,5-dimethoxy-1,4-phenylene)bis(ethane-2,1-diyl))bipyridine (PEBP-C4) and 4,4′-((1*E*,1′*E*)-(2,5-bis(octyloxy)−1,4-phenylene)bis(ethene-2,1-diyl))dipyridine (PEBP-C8) (Scheme 1), respectively. Using the highly oriented pyrolytic graphite (HOPG) as substrate could comprehend the interaction between molecules more purely. Combined with density functional theory (DFT) calculation, we further investigated the formation mechanism of the assembled systems. Our results will provide wider vision for the co-assembly of two-dimensional surface host-guest system.

The experimental methods were listed here. Sample preparation: BCDTDA and BP used in this experiment were purchased from Jilin Chinese Academy of Sciences, Yanshen Technology Co., Ltd., COR and 1-heptanoic acid was purchased from J&K Scientific. PEBP-C8 and PEBP-C4 were prepared as former reports [41], and all the chemical structures are shown in Scheme 1. The samples were used directly without further purification. Highly oriented pyrolytic graphite (HOPG) was used as a solid conductive substrate (grade ZYB, NTMDT, Russia). The concentrations of all solutions were lower than 10^{-4} mol/L. The HOPG was adhered with adhesive tape before the experiment to obtain a clean and smooth surface, and then the solutions were dropped on the substrate.

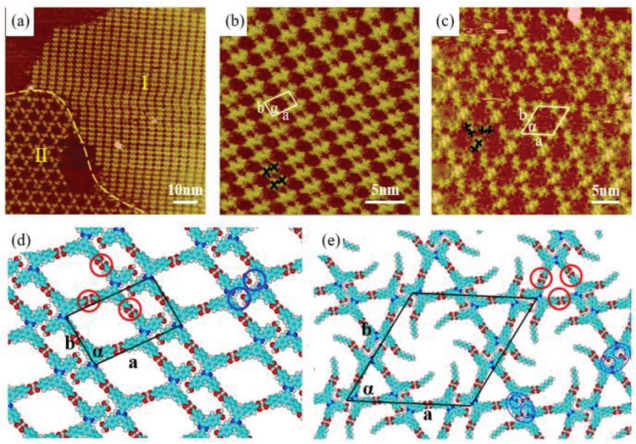

Fig. 1. (a) Large-scale (81.3 nm × 81.3 nm) STM image of BCDTDA self-assembled structure (I_{set} = 330 pA, V_{bias} = 700 mV). (b, c) High-resolution STM images of BCDTDA-I structure (25.0 nm×25.0 nm) (I_{set} = 299 pA, V_{bias} = 624 mV) and BCDTDA-II structure (36.2 nm × 36.2 nm) (I_{set}= 330 pA, V_{bias}= 700 mV). (d, e) Suggested molecular model for BCDTDA-I and BCDTDA-II structures, respectively.

Table 1
Experimental (Expt.) and calculated (Cal.) unit cell parameters for the assembled structures.

Sample		Unit cell parameters		
		a (nm)	*b* (nm)	*α* (°)
BCDTDA-I	Expt.	3.4 ± 0.2	2.0 ± 0.2	97 ± 1
	Cal.	3.40	2.01	98.0
BCDTDA-II	Expt.	5.9 ± 0.2	5.9 ± 0.2	60 ± 1
	Cal.	5.85	5.85	60.0
BCDTDA/COR	Expt.	5.9 ± 0.2	5.9 ± 0.2	60 ± 1
	Cal.	5.85	5.85	60.0
BCDTDA/BP	Expt.	3.7 ± 0.2	3.2 ± 0.2	106 ± 1
	Cal.	3.70	3.20	106.0
BCDTDA/PEBP-C4	Expt.	4.2 ± 0.2	3.5 ± 0.2	94 ± 1
	Cal.	4.20	3.50	94.0
BCDTDA/PEBP-C8-I	Expt.	3.5 ± 0.2	5.3 ± 0.2	107 ± 1
	Cal.	3.50	5.25	107.0
BCDTDA/PEBP-C8-II	Expt.	3.4 ± 0.2	3.6 ± 0.2	67 ± 1
	Cal.	3.40	3.60	67.0
BCDTDA/PEBP-C8-III	Expt.	3.5 ± 0.2	2.0 ± 0.2	76 ± 1
	Cal.	3.50	2.00	76.0

STM characterization and DFT calculations: The detail procedures were shown in Supporting information.

When the heptanoic acid (HA)-dissolved BCDTDA sample is dropped on HOPG surface, the large-scale STM image of the self-assembly structure of BCDTDA is obtained and shown in Fig. 1a. Two kinds of self-assembled structures, BCDTDA-I and BCDTDA-II, appeared in the surface when the concentration of BCDTDA is 1/8 saturated. During the entire observation process, the proportion of pattern I is larger than that of pattern II. However, when the concentration of BCDTDA is between 1/5 and 1/7 of saturated concentration, only BCDTDA-I can be observed. Therefore, experimentally, the self-assembly structure of BCDTDA-I is a more stable pattern. Fig. 1b shows that in the high-resolution STM image of BCDTDA-I, every two molecules formed a dimer which were represented by two black X-shaped patterns and every four dimers were arranged to form a rectangle cavity. Obviously, dimers as building blocks subsequently aggregated into long-range ordered nanolattice structures. The unit cell parameters of BCDTDA-I are calculated as $a = 3.4 \pm 0.2$ nm, $b = 2.0 \pm 0.2$ nm and $\alpha = 97° \pm 1°$ (Table 1).

DFT calculations have been performed to investigate the assembly mechanisms. In Fig. 1d, the theoretical model demonstrated

Table 2
Total energies and energies per unit area of the assemblies. Here, the more negative energy means the system is more stable.

Sample	Interactions between adsorbates (kcal/mol)	Interactions between adsorbates and substrate (kcal/mol)	Total energy (kcal/mol)	Energy per unit area (kcal mol^{-1} $Å^{-2}$)
BCDTDA-I	−101.615	−94.671	−196.286	−0.290
BCDTDA-II	−404.786	−386.487	−809.572	−0.273
BCDTDA/COR	−427.05	−445.699	−872.749	−0.294
BCDTDA/BP	−191.608	−180.721	−372.329	−0.327
BCDTDA/PEBP-C4	−197.665	−271.591	−469.256	−0.320
BCDTDA/PEBP-C8-I	−182.87	−346.212	−529.082	−0.301
BCDTDA/PEBP-C8-II	−92.711	−219.488	−312.199	−0.277
BCDTDA/PEBP-C8-III	−67.475	−115.668	−183.143	−0.270

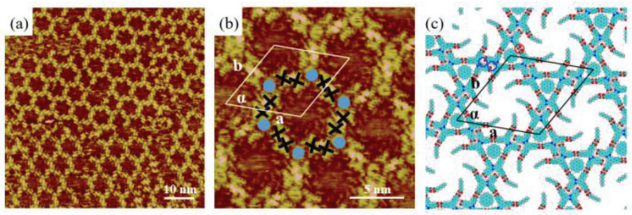

Fig. 2. (a) Large-scale (63.0 nm × 63.0 nm) STM image of the co-assembled structure of BCDTDA/COR. (b) High-resolution STM image of the co-assembly structure (16.8 nm × 16.8 nm) of BCDTDA/COR (I_{set} = 340 pA, V_{bias} = 693 mV). (c) Suggested molecular model for BCDTDA/COR co-assembly structure.

that a pair of N–H···O hydrogen bonds were formed through N–H of the imidazole group of BCDTDA and O atom of one carboxylic group of neighboring BCDTDA (blue circles in Fig. 1d), thus forming a hydrogen-bonded dimeric building block finally. Furthermore, the π-π interactions between the adjacent phenyl rings stabilized the dimers. Three remaining carboxyl groups of BCDTDA molecule were exposed to form O–H···O hydrogen bonds (red circles in Fig. 1d) with three neighboring BCDTDA molecules, and then they assembled into a regular tic-tac-toe grid structure.

The arrangement in pattern II is a well-ordered open network with an interesting Kagomé structure. In this pattern, the building blocks are still BCDTDA dimers. And every three dimers further head-to-tail formed a small triangular cavity (Fig. 1c) to compose the regular Kagomé structure with larger hexagonal cavities. Further theoretical molecular model is shown in Fig. 1e. It is noted that in BCDTDA-II, N–H···O hydrogen bonds in dimers keep existing (blue circles in Fig. 1e). And the adjacent three dimers formed the triangular cavity through O–H···O hydrogen bonding (red circles in Fig. 1e). The exposed carboxyl groups formed pairs of O–H···O hydrogen bonds with free solvent molecules to enhance the stability of self-assemblies on HOPG surfaces. The unit cell parameters of BCDTDA-II are calculated as $a = 5.9 \pm 0.2$ nm, $b = 5.9 \pm 0.2$ nm and $\alpha = 60° \pm 1°$ (Table 1).

DFT calculated parameters are also listed in Table 1, which agree well with the experimental values. The theoretical energies of the assemblies have been presented in Table 2, in which the total energy per unit area could be employed to compare the thermodynamic stability of the assemblies. Evidently, the total energy per unit area of BCDTDA-I is −0.290 kcal mol^{-1} $Å^{-2}$, which is lower than that of BCDTDA-II (−0.273 kcal mol^{-1} $Å^{-2}$). It indicates that BCDTDA-I is energetically more stable than BCDTDA-II, which is consistent with the experimental observation that BCDTDA-I has a higher proportion on the substrate surface.

After adding COR to the self-assembled structure formed by BCDTDA, both pattern I and pattern II structures formed the similar network which is shown in Fig. 2a. For BCDTDA-I, the introduction of COR induced the structural transformation of the assembly. While for BCDTDA-II, the basic Kagomé structure of the assembly seemed unchangeable, only COR molecules entered the small triangular cavities formed by three BCDTDA dimers. In Fig. 2b, the high-resolution STM image shows more details, in which two BCDTDA molecules still form one hydrogen-bonded dimer (marked with black X-shape), and COR molecules are captured inside the smaller triangular cavities (marked with blue dots). We have tried to increase the concentration of COR, but no COR molecules could be capsulated into the larger hexagonal cavities. We suggest that it possibly result from the spatial size matching effect. The lengths of edges of the triangular cavity are measured about 1.5 nm, while the diameter of the hexagonal cavity is approximately 4.5 nm. Considering that the diameter of COR is 0.9 nm, the triangular cavity is more suitable for the encapsulation of COR, and the hexagonal cavity is too large to fill COR. The unit cell is depicted and the parameters are: $a = 5.9 \pm 0.2$ nm, $b = 5.9 \pm 0.2$ nm and $\alpha = 60° \pm 1°$ (Table 1).

The experimental results were further confirmed by theoretical calculations in Fig. 2c, where the hydrogen bonding between BCDTDA molecules is the main driving force to stabilize the co-assembly structure. Every two BCDTDA molecules constituted N–H···O hydrogen-bonded dimer (blue circles in Fig. 2c). Each dimer interacted with the others through the similar O–H···O hydrogen bonding as that of BCDTDA-II (red circle in Fig. 2c). The exposed carboxyl groups of BCDTDA were perfectly combined with solvent molecules, which made the regular Kagomé structure more stable. And COR molecules were encapsulated in the triangular cavity by the π-π interaction between the benzene rings. The total energy per unit area of BCDTDA/COR is −0.294 kcal mol^{-1} $Å^{-2}$, which is lower than those of the self-assembled structures of BCDTDA molecules. Therefore, adding the COR molecules into the BCDTDA self-assembly structures makes the whole system more stable. However, the energy per unit area of BCDTDA/COR is close to that of BCDTDA-I (−0.290 kcal mol^{-1} $Å^{-2}$). This is the reason why the co-assembled structure is not long-range ordered in Fig. 2a.

After the self-assembled structure of BCDTDA-I is obtained under STM, the droplet of BP solution in HA is added. The large-scale and high-resolution STM images of BCDTDA/BP are shown in Figs. 3a and b, respectively. It can be seen from the STM image that BP molecules do not destroy the dimeric structure of BCDTDA, and the dimers marked with black X shapes are arranged side by side in rows. The adjacent BCDTDA dimers in neighboring rows are connected by two parallel BP molecules as bridges (marked with blue short lines). The unit cell parameters of BCDTDA/BP are: $a = 3.7 \pm 0.2$ nm, $b = 3.2 \pm 0.2$ nm, $\alpha = 106° \pm 1°$ (Table 1). Further DFT calculations have been performed, and the theoretical optimization model is presented in Fig. 3c.

Similar as the BCDTDA assemblies, in BCDTDA/BP co-assembly structure, two BCDTDA molecules still constructed a dimer by N–H···O hydrogen bonds (blue circles in Fig. 3c). Along axis b, only one pyridine group of BP molecules formed an O–H···N hydrogen

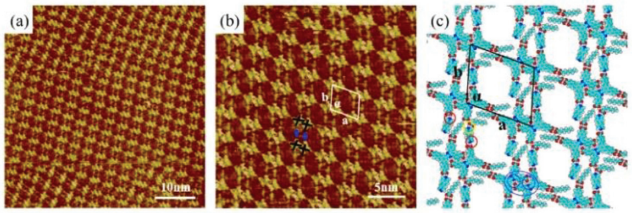

Fig. 3. (a) Large-scale (50.0 nm × 50.0 nm) STM image of the co-assembled structure of BCDTDA/BP. (b) High-resolution STM image of the co-assembly structure (26.9 nm × 26.9 nm) of BCDTDA/BP (I_{set} = 340 pA, V_{bias} = 693 mV). (c) Suggested molecular model for BCDTDA/BP.

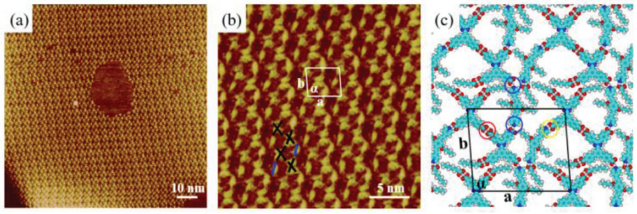

Fig. 4. (a) Large-scale (100.0 nm × 100.0 nm) STM image of BCDTDA/PEBP-C4 co-assembly structure. (b) High-resolution STM image of the co-assembly (25.0 nm × 25.0 nm) of BCDTDA/PEBP-C4 (I_{set} = 317 pA, V_{bias} = 700 mV). (c) Suggested molecular model for BCDTDA/PEBP-C4.

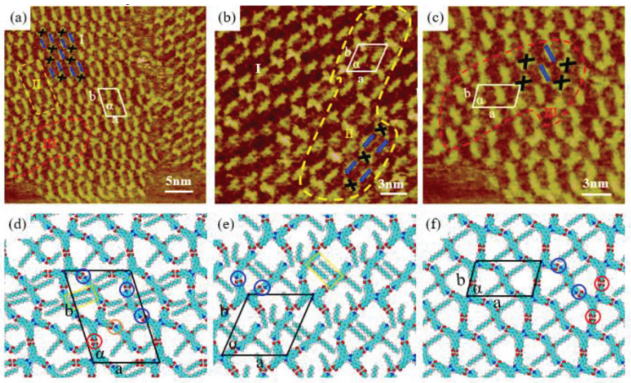

Fig. 5. (a) The STM image of BCDTDA/PEBP-C8-I assembly structure (35.7 nm × 35.7 nm). (b) STM image of BCDTDA/PEBP-C8-II assembly structure (22.6 nm × 22.6 nm). (c) STM image of BCDTDA/PEBP-C8-III assembly structure (18.0 nm × 18.0 nm) (I_{set} = 260 pA, V_{bias} = 700 mV). (d-f) Suggested molecular model for BCDTDA/PEBP-C8-I, BCDTDA/PEBP-C8-II and BCDTDA/PEBP-C8-III assembly structures, respectively.

bond with the neighboring dimers (shown in red circles). The solvent molecule HA constructed O–H···N hydrogen bond with one exposed pyridine group of BP molecule (shown in yellow circle) as the result of steric hindrance effect. It should be noted that the introduction of BP destroys the original O–H···O hydrogen bonds between the dimers of BCDTDA-I assembly structure. Such dislocation results in the vacancies of carboxyl groups of BCDTDA along axis a, which are exposed to facilitate the formation of O–H···O hydrogen bonding with the solvent HA. DFT results show that due to the introduction of BP, the total energy per unit area of BCDTDA/BP co-assembly structure (−0.327 kcal mol^{-1} Å^{-2}) is lower than that of BCDTDA-I assembly structure (Table 2). Therefore, we could observe the structural transformation of BCDTDA/BP assembly structure.

After obtaining BCDTDA-I self-assembly structure at the interface, the droplets of HA-dissolved PEBP-C4 and PEBP-C8 molecules are added, and the large-scale STM images of those co-assembly structures are obtained in Figs. 4a and 5a, respectively. Interestingly, in BCDTDA/PEBP-C4 and BCDTDA/PEBP-C8 assemblies, the N–H···O hydrogen bonded dimeric structure is destroyed, and each BCDTDA molecule interacted with pyridine molecules PEBP-C4 or PEBP-C8 individually. Fig. 4a shows that BCDTDA/PEBP-C4 is a long-range ordered co-assembled structure. From the high-resolution STM image in Fig. 4b, each unit cell contains two BCDTDA molecules (marked with black X-shaped patterns) and two PEBP-C4 molecules (marked with blue rods). The unit cell is depicted and the parameters are: $a = 4.2 \pm 0.2$ nm, $b = 3.5 \pm 0.2$ nm and $\alpha = 94° \pm 1°$ (Table 1).

To better explore the formation mechanism of the interwoven arrangement, DFT calculations have been performed and the optimized model is presented in Fig. 4c. DFT results show that every two BCDTDA molecules also form a dimer through a pair of O–H···O hydrogen bonds between the carboxyl groups (shown as red circle). Along axis *b* direction, one PEBP-C4 molecule acting as a bridge, connects with the neighbouring BCDTDA molecules in the adjacent dimers through O–H···N hydrogen bonds (shown as blue circles). In one unit cell, another PEBP-C4 molecule interacts with the carboxyl group of the other BCDTDA in the dimer by head-to-head O–H···N hydrogen bond which is circled in yellow. All the remaining exposed carboxyl groups of BCDTDA can form a pair of O–H···O hydrogen bonds with solvent molecules. And the remaining pyridine groups of PEBP-C4 can also form O–H···N hydrogen bonds with solvent molecules. Obviously, there are different exerted binding sites in the co-assembly due to the steric hindrance, so that the solvent molecules participate into the assembly to form hydrogen bonds.

For PEBP-C8, although PEBP-C8 is a bipyridine derivative with similar structure to PEBP-C4, the two-component co-assembly structure of BCDTDA/PEBP-C8 is quite different from BCDTDA/PEBP-C4 structure. Fig. 5a shows three assembled structures, BCDTDA/PEBP-C8-I, BCDTDA/PEBP-C8-II and BCDTDA/PEBP-C8-III, respectively, and the domain ratio of three structures is approximately 3:2:1. In the STM images, BCDTDA molecules are signed as black X-shaped patterns and PEBP-C8 molecules are signed as blue rods. In each domain, the molecular proportion for BCDTDA and PEBP-C8 molecules is 2:3, 1:2 and 1:1, respectively. DFT calculations have been carried out to investigate the formation mechanisms of three kinds of assemblies. The unit cell of BCDTDA/PEBP-C8-I is depicted in Fig. 5a, and the cell parameters are: $a = 3.5 \pm 0.2$ nm, $b = 5.3 \pm 0.2$ nm and $\alpha = 107° \pm 1°$ (Table 1).

Fig. 5d shows the DFT optimized molecular model for BCDTDA/PEBP-C8-I assembly. Every two BCDTDA molecules interact with each other to construct a dimer by forming double O–H···O hydrogen bonds between the carboxyl groups (shown as red circle). Two PEBP-C8 molecules, as bridges, head-to-tail connect the neighboring BCDTDA dimers by forming O–H···N hydrogen bonds (shown as blue circles), and the adjacent alkoxyl chains parallelly interact with each other by van der Waals interactions (shown as yellow rectangle). Due to the spatial limit and the steric hindrance, the left PEBP-C8 molecule interact with one BCDTDA by forming O–H···N hydrogen bond (shown as orange circle), and all the exposed binding sites (carboxyl groups or pyridine groups) interact with the solvent molecule by hydrogen bonds.

For BCDTDA/PEBP-C8-II assembly, the unit cell is depicted in Fig. 5b, and the parameters are: $a = 3.4 \pm 0.2$ nm, $b = 3.6 \pm 0.2$ nm and $\alpha = 67° \pm 1°$ (Table 1). Fig. 5e shows the DFT optimized model. In this case, each BCDTDA molecule, as a bridge, connects with two PEBP-C8 molecules and forms two O–H···N hydrogen bonds (shown as blue circles). Meanwhile, the alkoxyl chains between two PEBP-C8 molecules parallelly interact with each other by van der Waals interactions (shown as yellow rectangle). Similar to BCDTDA/PEBP-C8-I assembly, all the exposed binding sites (carboxyl groups or pyridine groups) interact with the solvent molecule by hydrogen bonds.

For BCDTDA/PEBP-C8-III assembly, the unit cell is depicted in Fig. 5c, and the parameters are: $a = 3.5 \pm 0.2$ nm, $b = 2.0 \pm 0.2$ nm and $\alpha = 76° \pm 1°$. It is the simplest co-assembled structure in these three co-assemblies, and the model is verified by DFT results in Fig. 5f. By forming O–H···O hydrogen bonds, each BCDTDA molecule head-to-tail interact with the other BCDTDA to aggregate into a row along axis *b* (shown as red circles). And one PEBP-C8 molecule acts as a bridge to connect two BCDTDA molecules in the neighboring rows through two O–H···N hydrogen bonds (shown as blue circles). Since there is no vacancy for binding sites, the solvent HA does not participate in this assembly.

According to DFT calculations, the total energy per unit area of BCDTDA/PEBP-C4 assembly is -0.320 kcal mol^{-1} Å^{-2}, which is lower than those of three structures of BCDTDA/PEBP-C8. It means that BCDTDA/PEBP-C4 assembly is more stable than the three structures of BCDTDA/PEBP-C8. Among the three structures of BCDTDA/PEBP-C8, the total energy per unit area of BCDTDA/PEBP-C8-I is lowest about -0.301 kcal mol^{-1} Å^{-2}, indicating BCDTDA/PEBP-C8-I is the most energetically stable structure. This also confirms the experimental observation that in the STM image the coverage of this structure is the largest. And the total energies per unit area of BCDTDA/PEBP-C8-II and BCDTDA/PEBP-C8-III were -0.277 kcal mol^{-1} Å^{-2} and -0.270 kcal mol^{-1} Å^{-2}, respectively, suggesting that although those structures exist on the two-dimensional surface, they are not stable, and thus with the less coverage in the STM image.

In this study, the assembly behaviors of BCDTDA with four carboxyl groups and one imidazole group, at the 1-heptanoic acid/HOPG interface, were investigated by STM and DFT calculations. Through N–H···O hydrogen bonding, two BCDTDA molecules form a dimeric structure as building blocks. Subsequently, the dimers are able to further aggregate into nanogrid structure (BCDTDA-I) and hexagonal structure (BCDTDA-II) by O–H···O hydrogen bonding, respectively. With the introduction of COR into the self-assembled structure, the nanogrid structure of BCDTDA-I was transformed into the similar Kagomé structure of BCDTDA-II, and the COR molecules could be captured in the small triangular cavities of BCDTDA-II. Different pyridine molecules (BP, PEBP-C4 and PEBP-C8) are selected to regulate the self-assembled structure of BCDTDA by forming O–H···N hydrogen bonds between the carboxylic groups and pyridine groups. For example, the addition of BP molecule did not destroy the dimer formed by BCDTDA molecule, while broke the O–H···O hydrogen bonds between the dimers, and BP acted as a bridge to connect two dimers by O–H···N hydrogen bonds. However, the introductions of PEBP-C4 and PEBP-C8 molecules broke the N–H···O hydrogen bonds of the dimers, while partially kept the O–H···O hydrogen bonds between BCDTDA molecules. The co-assembly of PEBP-C4 and BCDTDA were interwoven and staggered, which was stable and orderly. PEBP-C8 and BCDTDA formed three kinds of co-assembled structures. Obviously, different bipyridine molecules exhibit different regulatory effects on the dimer, which may destroy or retain the formation of the dimer, so that the system could be more stable. It also provides new reflections for the experimental assumption of dimer regulation.

Declaration of competing interest

The authors declare no conflict of interest.

Acknowledgments

This work was financially supported by the National Natural Science Foundation of China (Nos. 21972031, 12064026 and 22272039), the Strategic Priority Research Program of the Chinese Academy of Sciences (No. XDB36000000) and Jilin Chinese Academy of Sciences-Yanshen Technology Co., Ltd.

Supplementary materials

Supplementary material associated with this article can be found, in the online version, at doi:10.1016/j.cclet.2022.108005.

References

[1] X. Kang, M. Zhu, Coord. Chem. Rev. 394 (2019) 1–38.
[2] J. Huan, X. Zhang, Q. Zeng, Phys. Chem. Chem. Phys. 21 (2019) 11537–11553.
[3] J.M. Lehn, J. Incl. Phenom. Macrocycl. Chem. 6 (1988) 351–396.
[4] X. Peng, T. Meng, L. Wang, et al., Chin. Chem. Lett. 34 (2023) 107568.
[5] X. Li, J. Li, C. Ma, et al., Chin. Chem. Lett. 32 (2021) 1077–1080.
[6] Y. Xie, C. Liu, L. Cheng, et al., Chin. Chem. Lett. 33 (2022) 4649–4654.
[7] X. Peng, Y. Xiao, B. Mu, et al., Appl. Surf. Sci. 565 (2021) 150529.
[8] Z.Y. Yi, X.Q. Yang, J.J. Duan, et al., Nat. Commun. 13 (2022) 5850.
[9] J. Fang, X. Zhu, W. Luo, et al., Chin. Chem. Lett. 33 (2022) 1100–1104.
[10] Y. Xiao, F. Cai, X. Peng, et al., Chin. Chem. Lett. 32 (2021) 3566–3569.
[11] Y. Tobe, K. Tahara, S. De Feyter, Chem. Commun. 57 (2021) 962–977.
[12] S. Zhang, Y. Geng, Y. Fan, et al., Phys. Chem. Chem. Phys. 19 (2017) 31284–31289.
[13] S. Tan, J. Tao, W. Luo, et al., Chin. Chem. Lett. 32 (2021) 1149–1152.
[14] N.A. Wasio, R.C. Quardokus, R.P. Forrest, et al., Nature 507 (2014) 86–89.
[15] A. Mukherjee, J. Teyssandier, G. Hennrich, S. De Feyter, K.S. Mali, Chem. Sci. 8 (2017) 3759–3769.
[16] G. Velpula, M. Li, Y. Hu, et al., Chem. Eur. J. 24 (2018) 12071–12077.
[17] J. Xu, Q.D. Zeng, Chin. Chem. Lett. 24 (2013) 177–182.
[18] X. Qiu, C. Wang, Q. Zeng, et al., J. Am. Chem. Soc. 122 (2000) 5550–5556.
[19] W. Li, X. Leng, C. Xu, N. Liu, Phys. E: Low Dimens. 101 (2018) 197–200.
[20] X. Li, S. Zhang, J. Li, et al., New J. Chem. 43 (2019) 13315–13325.
[21] K. Iritani, K. Tahara, S. De Feyter, Y. Tobe, Langmuir 33 (2017) 4601–4618.
[22] K. Miao, Y. Hu, B. Zha, et al., J. Phys. Chem. C 120 (2016) 14187–14197.
[23] D.D. Feng, Y.D. Zhao, X.Q. Wang, et al., Dalton. Trans. 48 (2019) 10892–10900.
[24] D. Xue, L. Ma, Y. Tian, et al., Front. Chem. 9 (2021) 707232.
[25] T. Meng, Y. Lu, P. Lei, et al., Langmuir 38 (2022) 3568–3574.
[26] S. De Feyter, F.C. De Schryver, Chem. Soc. Rev. 32 (2003) 139–150.
[27] L. Verstraete, S. De Feyter, Chem. Soc. Rev. 50 (2021) 5884–5897.
[28] L. Verstraete, J. Smart, B.E. Hirsch, S. De Feyter, Phys. Chem. Chem. Phys. 20 (2018) 27482–27489.
[29] Q. Xue, Y. Zhang, R. Li, et al., Chin. Chem. Lett. 30 (2019) 2355–2358.
[30] C. Lu, Y.P. Mo, Y. Hong, et al., J. Am. Chem. Soc. 142 (2020) 14350–14356.
[31] A. Gowda, L. Jacob, A. Patra, et al., Dyes. Pigments 160 (2019) 128–135.
[32] H.Q. Dong, T.B. Wei, X.Q. Ma, et al., J. Mater. Chem. C 8 (2020) 13501–13529.
[33] N. Devi, R.K. Rawal, V. Singh, Tetrahedron 71 (2015) 183–232.
[34] C. Ma, J. Li, S. Zhang, W. Duan, Q. Zeng, Nanotechnology 32 (2021) 382001.
[35] C. Lu, Y. Li, L.M. Wang, et al., Chem. Commun. 55 (2019) 1326–1329.
[36] C. Zeng, H. Wang, B. Wang, J. Yang, J.G. Hou, Appl. Phys. Lett. 77 (2000) 3595–3597.
[37] J. Liu, X. Zhang, H.J. Yan, et al., Langmuir 26 (2010) 8195–8200.
[38] J. Li, B. Tu, X. Li, et al., Chem. Commun. 55 (2019) 11599–11602.
[39] X. Peng, L. Cheng, X. Zhu, et al., Nano Res. 11 (2018) 5823–5834.
[40] S. Zhang, C. Chen, J. Li, et al., Nanoscale 14 (2022) 2419–2426.
[41] S. Bhattacharjee, S. Bhattacharya, Chem. Commun. 51 (2015) 7019–7022.